Eur. Phys. J. A **14**, 137–146 (2002)
DOI 10.1140/epja/i2002-10005-1

THE EUROPEAN PHYSICAL JOURNAL A

High-resolution in-beam particle spectroscopy —New results on prompt proton emission from ^{58}Cu

D. Rudolph[1,a], D.G. Sarantites[2], C. Andreoiu[1], C. Fahlander[1], D.P. Balamuth[3], R.J. Charity[2], M. Devlin[2,b], J. Eberth[4], A. Galindo-Uribarri[5], P.A. Hausladen[3,c], D. Seweryniak[6], L.G. Sobotka[2], and Th. Steinhardt[4]

[1] Department of Physics, Lund University, S-22100 Lund, Sweden
[2] Chemistry Department, Washington University, St. Louis, MO 63130, USA
[3] Department of Physics and Astronomy, University of Pennsylvania, Philadelphia, PA 19104, USA
[4] Institut für Kernphysik, Universität zu Köln, D-50937 Köln, Germany
[5] Physics Division, Oak Ridge National Laboratory, Oak Ridge, TN 37831, USA
[6] Physics Division, Argonne National Laboratory, Argonne, IL 60439, USA

Received: 11 March 2002 / Revised version: 4 April 2002
Communicated by D. Schwalm

Abstract. Prompt proton decay lines in ^{58}Cu have been studied by means of high-resolution in-beam particle-γ coincidence spectroscopy using the GAMMASPHERE Ge-detector array in conjunction with a dedicated set of ancillary detectors including four ΔE-E silicon-strip telescopes. High-spin states in ^{58}Cu have been populated via the heavy-ion fusion-evaporation reaction ^{28}Si(^{36}Ar, $1\alpha 1$p1n) at 148 MeV beam energy. The full-width at half maximum for the proton peak could be reduced significantly compared to earlier experiments. The results indicate that only one prompt proton decay branch exists in the decay-out of the well-deformed band of ^{58}Cu.

PACS. 23.20.Lv Gamma transitions and level energies – 23.50.+z Decay by proton emission – 27.40.+z $39 \leq A \leq 58$

1 Introduction

In proton-rich nuclei in the vicinity of ^{56}Ni a new nuclear decay mode called prompt particle emission has been established during recent years. The first case of prompt proton emission from excited high-spin states in the well-deformed second minimum of the nuclear potential into spherical daughter states had been identified in ^{58}Cu [1]. In the following, additional prompt proton decays have been found in ^{56}Ni [2] and ^{59}Cu [3,4], and a case of prompt α-particle emission has been observed in ^{58}Ni [5].

The decay mode is called "prompt", because the formation of the residual nucleus, the γ-decay of the rotational band in the second minimum, the particle emission, and finally the γ-decay in the daughter nucleus are observed in "prompt" coincidence in thin-target in-beam fusion-evaporation experiments, which have a typical observation time window of less than three nanoseconds. Thereafter, the recoiling nuclei have left both the focus of the Ge-detector array and the charged-particle detection system surrounding the target position. The particle decays compete with the conventional γ-decay-out, and they may be viewed as self-regulated two-dimensional quantum tunneling processes: The problem is two dimensional, because the initial states are prolate deformed with a long-to-short axis ratio of about 1.5:1 (see, *e.g.*, refs. [1,6]). The process is self-regulated, because the emission of the particles induces a drastic rearrangement of the nuclear mean-field potential, since the final states are spherical or even slightly oblate deformed. In fact, the shape change associated with the decay mode seems to cause major problems in the theoretical description of the process, though proton decay rates from spherical-to-spherical or deformed-to-deformed states are well understood based on significant recent advances in the theoretical modelling (see, *e.g.*, refs. [7–11] and references therein). In turn, the experimental knowledge concerning the prompt proton decays has been increased systematically following the first observation of the decay mode [1]. The focus has been on ^{58}Cu, where spins and parities of the initial and final state could be assigned [6,12] and lifetimes of γ- and proton-decaying states have been measured in the decay-out regime of the rotational band [6,13].

[a] e-mail: Dirk.Rudolph@kosufy.lu.se
[b] *Present address*: LANSCE-3, Los Alamos National Laboratory, Los Alamos, NM 87545, USA.
[c] *Present address*: Physics Division, Oak Ridge National Laboratory, Oak Ridge, TN 37831, USA.

This study presents further experimental results concerning the prompt proton decay in ^{58}Cu. Here, we focus on the previously suggested weak proton decay branches into the 3864 keV $11/2^-$ state in ^{57}Ni [1]. The following section (sect. 2) provides the details of a dedicated experiment aiming at high-resolution in-beam particle-γ coincidence spectroscopy, *i.e.* the search for weak fine-structure particle branches for the previously known cases [1–3, 5] as well as the identification of new particle-decaying states [4]. Section 3 describes the analysis and results for ^{58}Cu, which are subsequently discussed in sect. 4.

2 Experiment

The experiment was performed at the Argonne Tandem Linac Accelerator System ATLAS at the Argonne National Laboratory. High-spin states in ^{58}Cu were populated using the fusion-evaporation reaction ^{28}Si(^{36}Ar, 1α1p1n) at 148 MeV beam energy. The 0.4 mg/cm^2 thin target layer of 99.1% enriched ^{28}Si was sputtered onto a 1.0 mg/cm^2 gold support foil. The gold foil faced the beam and led to a reduction of some seven MeV in-beam energy for reactions on ^{28}Si. The GAMMASPHERE array [14] consisted of 86 Compton-suppressed germanium-detector elements. The heavimet collimators were removed to collect event-by-event γ-ray sum energy, H, and multiplicity, K, information. The most forward section of GAMMASPHERE had been replaced by twenty liquid-scintillator neutron detectors, and evaporated charged-particle detectors were detected in MICROBALL [15] and a wall of four ΔE-E silicon-strip telescopes [16,17]. These telescopes replaced the forward three rings of MICROBALL in the beam (z) direction, which normally comprise 28 CsI detector elements. Figure 1 presents a schematic drawing of the set-up.

Each of the four silicon telescopes consisted of a ΔE counter with a thickness of ~ 65 μm followed by an E detector of ~ 1 mm. Each of the eight elements was 50 mm $\times$ 50 mm in size and electrically separated into 16 strips. The strips of the ΔE detectors run in vertical direction (x), while those of the E detectors were arranged horizontally (y). This gives rise to a maximum of $4 \times 16 \times 16 = 1024$ pixels of 3 mm $\times$ 3 mm size. Due to the geometrical limit set by the fourth ring of MICROBALL, which covers the azimuthal-angle range of $44^\circ < \theta < 60^\circ$ [15] some 800 pixels were available for particles coming from the reaction spot. A simplified scheme of the silicon-strip detectors is shown in fig. 2. Part (a) shows a vertical cut through the system, with the beam entering from the left. The distance d from the target to the middle of the ΔE-E telescopes at $\theta = 0^\circ$ was 6.6(1) cm, and the telescopes were tilted relative to the (x,y)-plane by an angle $\alpha = 4.0(3)^\circ$ (see below). The numbers on the right-hand side of fig. 2(a) indicate the telescope identification number. They are also given in fig. 2(b). That part of the figure provides the (x,y)-plane of the silicon-strip telescopes perpendicular to the beam direction. The parameters $a = 1.0(1)$ cm and $b = a - 0.3$ cm indicate the (equal) offset of all four telescopes from the origin of the coordinate system. The knowledge of a, d, and α allows for the determination of the angles θ_i and ϕ_i for the center of each individual pixel. These angles are necessary for the proper transformation of the measured energies ($E_{\rm lab}$) and momenta of detected protons and α-particles into the center-of-mass ($E_{\rm p,cm}$) system according to

$$E_{\rm p,cm} = E_{\rm lab} + E_{\rm kin} - 2\sqrt{E_{\rm lab}E_{\rm kin}}\cos\Theta. \qquad (1)$$

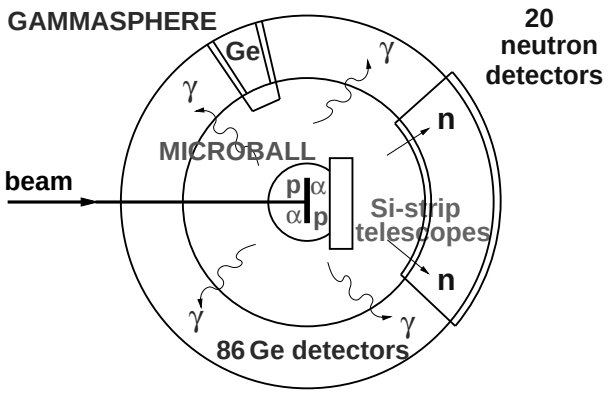

Fig. 1. Schematic view of the experimental set-up.

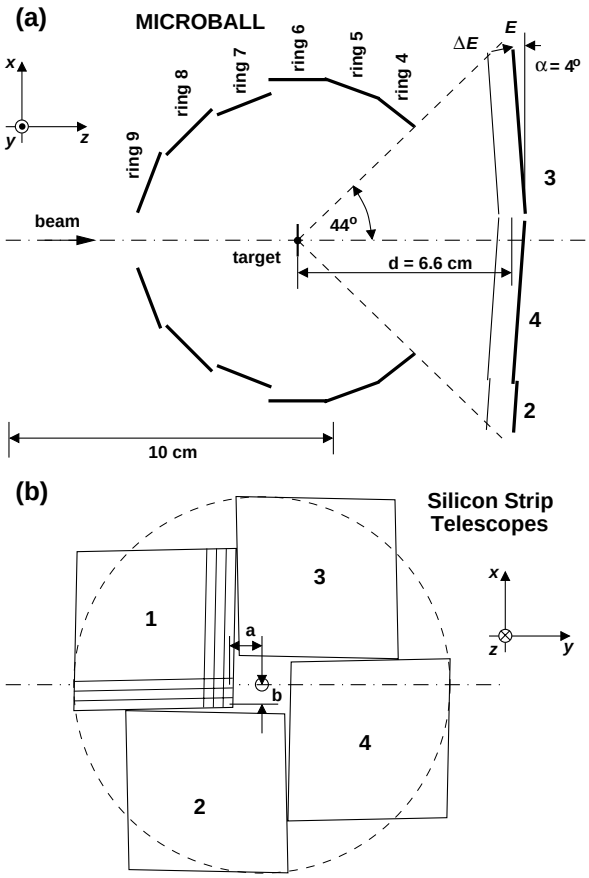

Fig. 2. Simplified side (part (a)) and front (part (b)) view of the silicon-strip detector set-up. See text for details.

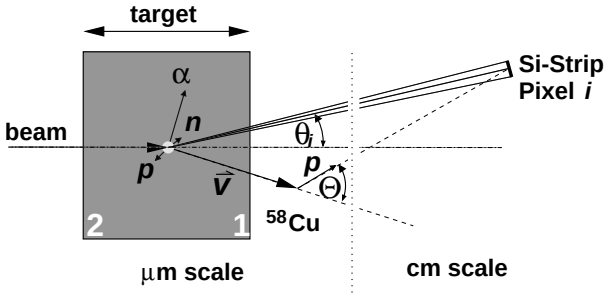

Fig. 3. Sketch of geometric and kinematic contributions to the resolution of proton lines for the present in-beam set-up.

$E_{\rm kin}$ denotes the kinetic energy of the proton at the time of the emission from the ^{58}Cu nucleus, and Θ is the angle between the momentum vector of the ^{58}Cu recoil and the Si-strip element i situated at θ_i, ϕ_i, which detects the proton (see fig. 3).

There are several contributions to the resolution of the prompt proton lines:

1. The combined intrinsic resolution of the ΔE and E detectors.
2. The energy spread due to the thin (~ 30 mg/cm^2) Pb absorbers.
3. The uncertainty in the knowledge of θ_i and ϕ_i.
4. The finite opening angle $\Delta\theta_i$ of a single pixel.
5. The beam diameter and the position stability of the beam spot.
6. The uncertainty in the direction of the recoil velocity.
7. The uncertainty in the magnitude of the recoil velocity.
8. The unknown precise depth of the reaction in the target.

Contributions 1 and 2 affect the quantity $E_{\rm lab}$ in eq. (1), while contributions 3, 4, 5, and 6 mainly act on the angle Θ. Contributions 7 and 8 lead to uncertainties in the knowledge of $E_{\rm kin}$.

Three calibrations of the silicon-strip telescopes (and the MICROBALL elements) were performed directly after the experiment: The reaction ^{12}C(p, p′) was used at 11.962 MeV with and without the Pb absorber foils, and a calibration was performed with a ^{228}Th α source (no absorber foils). The latter allows to calibrate the 64 ΔE strips in the energy range between some 5 MeV and 10 MeV with linear functions. The (p, p′) reaction (no absorbers) can subsequently be used to deduce offset and gain coefficients for all 64 ΔE strips ($E < 1$ MeV) and 64 E strips (a total of 256 parameters), since it provides some $2 \times 800 = 1600$ peak positions of the elastic and inelastic ($Q = 4.439$ keV) scattering on ^{12}C in ΔE plus E sum energy spectra for each of the ~ 800 active pixels. The fact that the energy of the scattered protons is angle dependent allows to include three more parameters in the least squares fitting procedure, namely the geometric quantities a, d, and α mentioned earlier. The result is the spectrum in fig. 4(a), which is the summed spectrum of all active pixels using the calibration coefficients and geometric parameters obtained from the least squares fit. The peak positions are at 7.523 MeV and 11.963 MeV

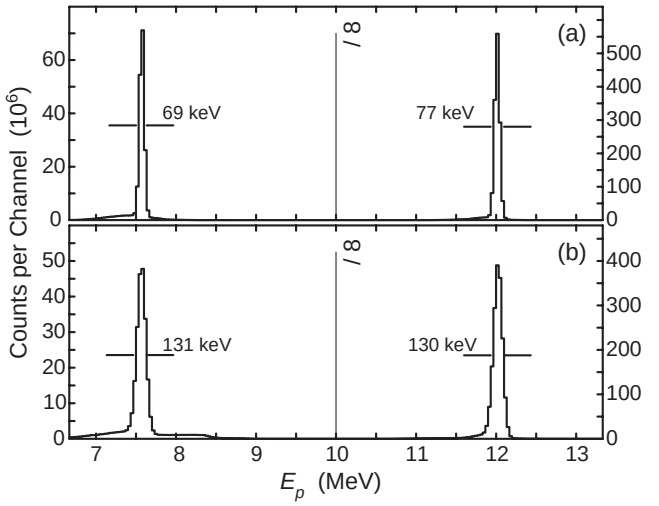

Fig. 4. Sum of calibrated proton spectra of about 800 active pixels in the Si-strip telescopes following the reaction ^{12}C(p, p′). For each pixel, the sum energy of the corresponding calibrated ΔE and E strips is used. Part (a) has been measured without any absorber foils. The data for part (b) has been taken with ~ 30 mg/cm^2 thin lead absorber foils in front of the detectors. The spectrum is corrected for the energy loss of the protons in the absorber foils. The FWHM are given in keV, and the energy calibration is 33.33 keV per channel. See text for more details.

with full-widths at half maximum (FWHM) of 69 keV and 77 keV, respectively.

During the experiment it is necessary to use thin foils to protect the Si-strip detectors from direct hits of beam particles. For the present experiment Pb foils were used with an approximate thickness of ~ 30 mg/cm^2. The effective thickness in front of *each individual* pixel can be determined from the different peak positions of the (p, p′) reaction in calibrated ΔE plus E sum energy spectra when running the reaction with or without the absorber foils. A semi-empirical function $E_{\rm lab} = f(E_{\rm det}, D)$ has been derived using results of stopping-power simulations obtained with the code TRIM96 [18]. This provides the proton energy in the laboratory frame $E_{\rm lab}$ as a function of the detected proton energy $E_{\rm det}$ measured after passing through the Pb absorber foil with the thickness D for the respective pixel. The formula was optimized for proton energies of 3 MeV $< E_{\rm lab} <$ 20 MeV and thicknesses D of Pb foils ranging from 25 to 35 mg/cm^2. In the calibration, both $E_{\rm lab}$ and $E_{\rm det}$ are known. Thus, D can be determined pixel by pixel. Figure 4(b) shows the final spectrum for the ^{12}C(p, p′) calibration run *including* the absorber foils. The peak positions are at 7.517 and 11.973 MeV, *i.e.* only slightly off from the nominal numbers (see above). This is well accounted for in the final results by adding a 10 keV systematic uncertainty to the proton center-of-mass energies. The FWHM increases from some 70–80 keV to $\Delta E_{\rm cal} = 130$ keV due to the energy straggling in the absorbers.

The second class of contributions to the resolution of the in-beam experiment arises from the geometric limits

(nos. 3–5 in the list above). The finite opening angle of the CsI elements of MICROBALL turned out to give the largest contribution to the FWHM of the proton peaks observed so far [1–3]. For example, the detectors in the MICROBALL ring 2 cover the azimuthal angular range of $14° < \theta < 28°$ [15]. If one plugs typical numbers of $E_{\rm lab} = 6.25$ MeV and $E_{\rm kin} = 1.25$ MeV into eq. (1), protons with center-of-mass energies of 2.08 MeV and 2.56 MeV could correspond to hits at 14° and 28° in the *same* element, *i.e.* they are not distinguishable. In fact, this aspect led us to replace the forward section of MICROBALL with the highly segmented Si-strip arrangement. The pixels of the present set-up provide values of only $\Delta\theta_i \sim 2.5°$, which reduces the respective energy spread from up to 500 keV to about 80 keV. In turn, the beam diameter and/or the stability of the beam position during the whole time span of the experiment becomes important. If the combined uncertainty of these two beam parameters were less than only 2 mm, the effective opening angle of a single pixel would increase from the nominal $\Delta\theta_i \sim 2.5°$ to $\Delta\theta_i \sim 4.5°$. This may increase the ideal energy spread of 80 keV to a realistic number of about $\Delta E_{\rm geo} \sim 150$ keV, including also the uncertainties in the positioning of the Si-strip array (see above).

Kinematic effects have also to be accounted for. Important parameters are both the direction and the magnitude of the velocity (or momentum) vector of the proton-emitting recoil and, related to the latter, the reaction point in the target. If the measurement were exclusive, *i.e.* if one knows the beam energy precisely and detects the energies and directions of all evaporated particles event by event, the momentum vector and initial energy of the recoil could be deduced. In practice, this is only approximately possible. The direction of the momentum vector is known reasonably well, because of the efficient measurement of the evaporated particles. However, the magnitude of the vector is difficult to determine on an event-by-event basis, because i) it is impossible to say whether a reaction took place at the beginning or at the end of the thin target layer, and ii) relatively large systematic uncertainties are associated with the energy loss simulation of the recoiling nuclei in the remaining target material, *i.e.* after their formation but before the prompt proton emission takes place (see fig. 3). A reaction at the end of the target (point "1" in fig. 3) takes place with a reduced beam energy due to energy losses of the beam particles in the target. Nevertheless, the recoil does not lose kinetic energy until it emits the particle, and $E_{\rm kin} = 1.22$ MeV can be estimated for such a case with TRIM96 [18] simulations. A reaction at the beginning of the target, however, takes place with the nominal beam energy, but the recoil loses energy in the whole 0.5 mg/cm^2 target foil, leading to $E_{\rm kin} = 1.03$ MeV. For a given (corrected, see above) energy $E_{\rm lab} = 6.25$ MeV detected at a given angle $\Theta = 21°$ (see fig. 3) one obtains $E_{\rm p,cm} = 2.31$ MeV and 2.54 MeV for the two cases, respectively. Thus, one can expect a contribution of $\Delta E_{\rm kin} \sim 230$ keV to the FWHM, which is mainly due to the finite target thickness.

In total, one thus expects a proton energy resolution of

$$\Delta E_{\rm p,cm} \sim \sqrt{\Delta E_{\rm cal}^2 + \Delta E_{\rm geo}^2 + \Delta E_{\rm kin}^2} = 300 \text{ keV} \quad (2)$$

for the present in-beam particle decay study. It appears that the only significant improvement for future experiments of this kind lies in the reduction of the target thickness by about a factor of two, which may yield $\Delta E_{\rm p,cm} \sim 250$ keV.

3 Analysis and results in ^{58}Cu

3.1 $\gamma\gamma$ coincidence analysis

The known high-spin excitation scheme of ^{58}Cu [1,6,19] has been revisited on the basis of the present data set by means of standard high-spin γ-ray analysis techniques. The RADWARE analysis software [20] and the spectrum analysis code TV [21] were used to investigate γ-ray coincidences, intensities, and angular correlations. The analysis was performed with γ-ray spectra and $\gamma\gamma$ matrices, which were gated by one α-particle, one neutron, and zero or one proton. In addition, only those events were selected which had proper γ-ray sum energy and multiplicity and charged-particle sum energy correlations. The result is the level scheme shown in fig. 5. Three modifications have been inferred as compared to the previous publications [1,19]: First of all, two transitions have been added, namely one at 1818 keV connecting the 7392 keV (11^+) and 5574 keV (9^+) states, and tentatively the high-energy 4399 keV (11^+) $\rightarrow$ 9^+ linking transition between

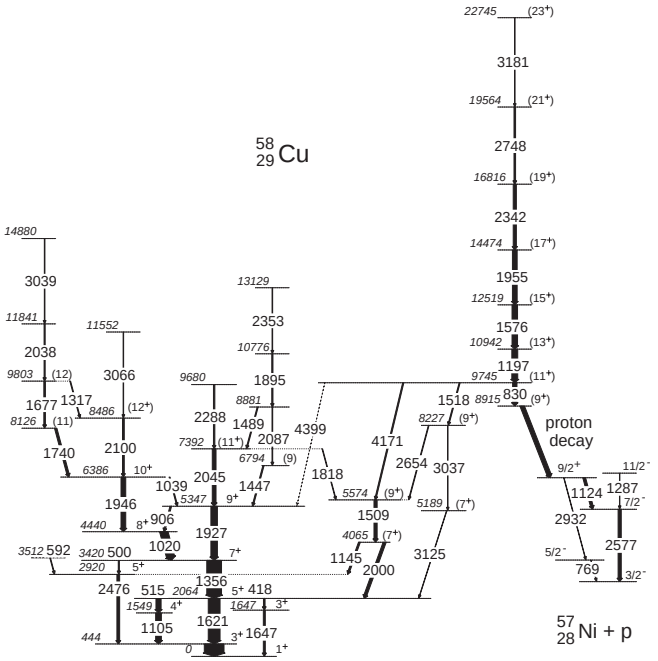

Fig. 5. Proposed partial decay scheme of ^{58}Cu including the proton decay into states of ^{57}Ni. The labels are in keV and the widths of the arrows representing the γ-ray transitions correspond to their relative intensities.

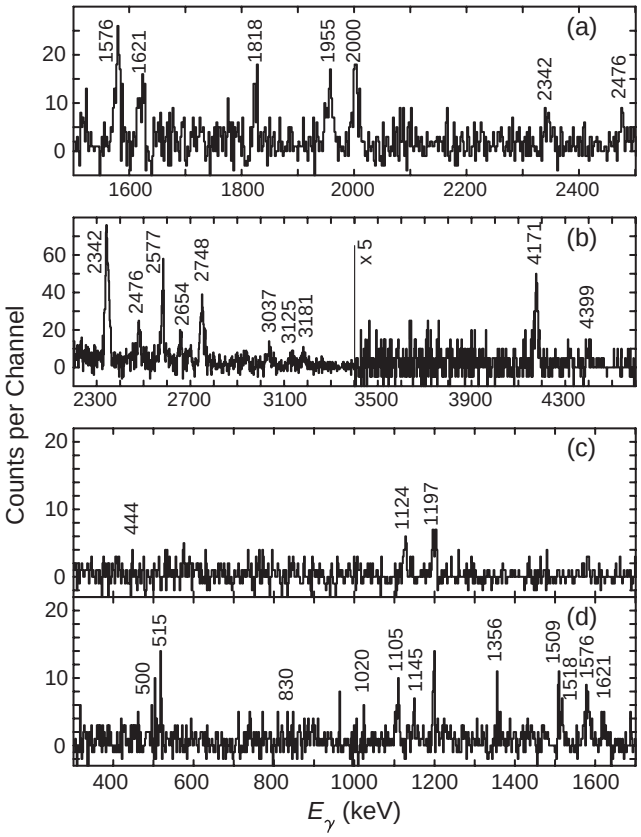

Fig. 6. Gamma-ray spectra of ^{58}Cu obtained from a $\gamma\gamma$ matrix and a $\gamma\gamma\gamma$ cube gated by one α-particle, one neutron, and zero or one proton. Part (a) is in coincidence with the 1509 keV $(9^+) \rightarrow (7^+)$ transition. Parts (b), (c), and (d) are in coincidence with the 1197, 1576, 1955, 2342, or 2748 transition, which form the major portion of the rotational band. In addition, parts (c) and (d) are in coincidence with a second γ at 830 keV (rotational band) or 444 keV (ground-state transition), repsectively. The energy labels are in keV, and the spectra have a resolution of 2 keV per channel.

the 9745 keV state in the rotational band and the level at 5347 keV situated in the spherical minimum. The transitions have relative intensities of 3(1) and 1(1) in the units of ref. [19], respectively. The evidence for their presence in the level scheme is presented in the γ-ray spectra of figs. 6(a) and (b). There are fourteen counts in eight channels for the tentative 4399 keV high-energy transition, while at most three background counts are expected in that part of the spectrum. Weak peaks at 1020, 1356, and 1927 keV are present in the corresponding low-energy part of the spectrum in fig. 6(b), which further support the 4399 keV connection. All four γ-ray spectra in fig. 6 have been gated by one α-particle, zero or one proton, and one neutron, which were detected in either MICROBALL, the Si-strip array, or the neutron detectors, respectively. The spectrum in fig. 6(a) is in coincidence with the 1509 keV $(9^+) \rightarrow (7^+)$ transition, while for part (b) a coincidence with either the 1197, 1576, 1955, 2342, or 2748 transition has been demanded. Secondly, the presence of the previously tentative 3037 and 3125 keV lines could be confirmed (see fig. 6(b)). Finally, the 1396, 2330, and 3073 keV transitions, which were suggested [1] to form a γ-decay branch from the lowest state observed in the rotational band, cannot be seen in fig. 6(b). This is in line with the remaining two spectra displayed in fig. 6, which are in double coincidence with one of the above-mentioned band members and the 830 keV transition at the bottom of the band (panel (c)) or the 444 keV ground-state transition (panel (d)), respectively. The absence of a peak at 444 keV in fig. 6(c) and the absence of a peak at 830 keV in fig. 6(d) indicate that any potential connection between the 8915 keV state in the rotational band and the other parts of the level scheme of ^{58}Cu has to be extremely weak. Comparing the number of counts at 444 keV and 1124 keV in fig. 6(c) and the number of counts at 830 keV and 1197 keV in fig. 6(d) it is possible to derive upper limits of possible γ-decay branches from the 8915 keV state of 11% and 7%, respectively.

Angular correlations between γ-rays detected in the detectors situated at backward angles ($\overline{\Theta} = 150°$) and the central section ($\overline{\Theta} = 97°$) of GAMMASPHERE were investigated by means of DCO ratios [22]:

$$R_{\rm DCO}(\gamma_1, \gamma_2) = \frac{I(\gamma_1 \text{ at } 150°;\ \text{gated with } \gamma_2 \text{ at } 97°)}{I(\gamma_1 \text{ at } 97°;\ \text{gated with } \gamma_2 \text{ at } 150°)}\,. \quad (3)$$

The numbers presented in table 1 are corrected for detection efficiencies. It should be noted that for fusion-evaporation reactions the γ-ray angular distributions and correlations are symmetric to the plane perpendicular to the beam axis, *i.e.* eq. (3) is identical to eq. (2) in ref. [19]. Due to the similarities in Ge-detector angles, the results from eq. (3) are also comparable to those obtained from eq. (1) in ref. [6]. Hence, the right $R_{\rm DCO}$ column in table 1 presents the average values from the independent previous and present DCO-ratio analyses. The numbers in table 1 as well as the newly identified γ-ray transitions at 1818 and 4399 keV strongly support the tentative (9^+) assignments to the levels at 5574, 8227, and 8915 keV and the tentative (11^+) assignment to the 9745 keV state. The

Table 1. Gamma-ray energies E_γ in keV, angular-correlation ratios $R_{\rm DCO}$, and multipole assignments for selected transitions in ^{58}Cu. The $R_{\rm DCO}$ column to the right gives the mean values from the present analysis (cf. eq. (3)) and refs. [6,19].

E_γ	$R_{\rm DCO}$		Mult.	$I_{\rm i}$ ($\hbar$)	$I_{\rm f}$ ($\hbar$)
830	0.96(18)	0.94(10)	$E2$	(11^+)	(9^+)
1197	0.89(15)	1.00(10)	$E2$	(13^+)	(11^+)
1576	1.23(21)	0.99(8)	$E2$	(15^+)	(13^+)
1955	0.89(16)	1.00(10)	$E2$	(17^+)	(15^+)
2342	1.16(20)	1.15(15)	$(E2)$	(19^+)	(17^+)
1124	0.49(11)	0.55(7)	$E1$	$9/2^+$	$7/2^-$ (^{57}Ni)
1145	0.85(31)	0.90(15)	$(E2)$	(7^+)	5^+
1509	0.91(39)	1.00(15)	$(E2)$	(9^+)	(7^+)
1518	0.95(41)	1.01(15)	$(E2)$	(11^+)	(9^+)
2000	0.87(28)	0.90(21)	$(E2)$	(7^+)	5^+
4171	1.06(32)	1.13(26)	$(E2)$	(11^+)	(9^+)

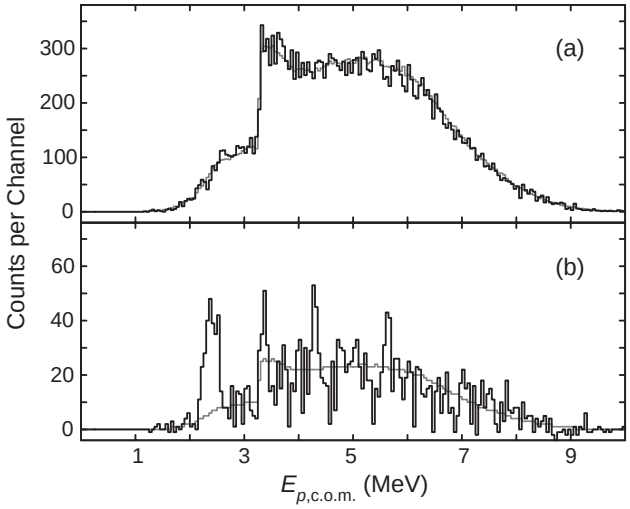

Fig. 7. Proton center-of-mass energy spectra of ^{58}Cu obtained from a proton-γ coincidence matrix. Panel (a) is in coincidence with the 1287 keV transition and panel (b) is in coincidence with the 1124 keV transition in ^{57}Ni. The grey lines indicate the "background" from evaporated protons. The resolution of the spectra is 50 keV per channel.

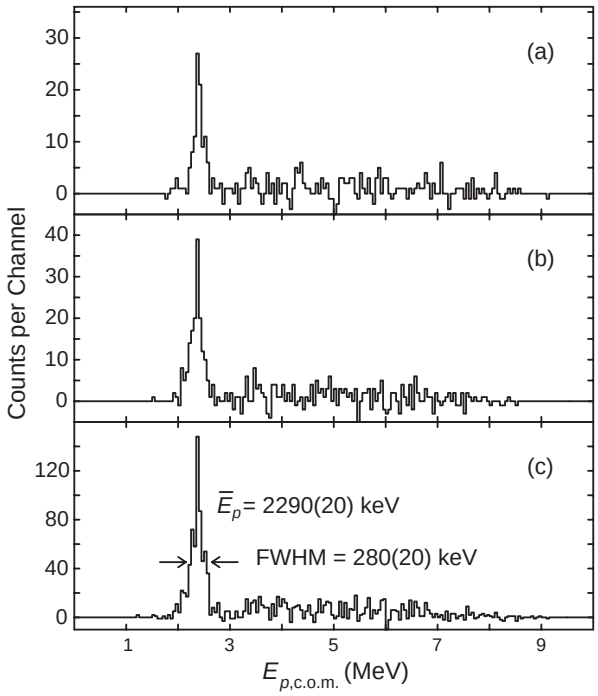

Fig. 8. Proton center-of-mass energy spectra of ^{58}Cu obtained from a proton-$\gamma\gamma$ coincidence cube. One coincident γ-ray has to be a given member of the rotational band in ^{58}Cu, while the second coincident γ-ray is the 1124 keV transition in ^{57}Ni for panel (a), the 830 keV transition at the bottom of the ^{58}Cu band for panel (b), and any (different) band member in the case of panel (c). See text for further details.

tentative spin assignments on top of the band are based on the regular rotational behaviour of the structure.

3.2 Proton-γ coincidence analysis

The study of coincidences between γ-ray transitions and discrete-energy proton lines from the new decay mode requires a dedicated treatment in the off-line analysis. Usually, for a given event all particles that have been detected in the ancillary detector systems are considered to be evaporated particles, since it is impossible to associate them with the very rare prompt particle decay mode without a more thorough investigation of the event as a whole. This assumption, of course, leads to a false treatment of events which do involve protons from the new decay mode (see fig. 3): Gamma-ray transitions are associated with the wrong reaction channel, the vector of the recoil is incorrect, but most importantly the center-of-mass proton energy is wrongly calculated, because for evaporated particles θ_i is used instead of Θ (cf. fig. 3 and eq. (1)). The angle Θ must be used for the protons from the prompt particle decays to obtain the best possible energy resolution.

The first task is therefore to identify the rare events, which are good candidates for prompt proton decays from a certain structure, *i.e.* in the present case from the deformed band in ^{58}Cu into final states of ^{57}Ni. The compromise between pure reaction channel selection and the amount of statistics implies that one α-particle, one or two protons, and one neutron need to be part of the event. In addition, correlations between the measured sum of the particle energies E_{part}, the sum of γ-ray energies, H, and the γ-ray multiplicity, K had to pass conditions being compatible with the final formation of ^{57}Ni residues [23]. It is, of course, necessary that at least one proton has to be detected in one of the four Si-strip detectors. From the known masses of ^{58}Cu and ^{57}Ni and the known γ-ray transition energies $Q_{\mathrm{p}} = 2.341(5)$ MeV can be derived for the main known proton branch in ^{58}Cu [1]. To allow for a search of weak, new proton branches within a reasonable energy window an upper threshold of $E_{\mathrm{p,cm}} < 3.2$ MeV has been inferred. The energy of the proton detected in the Si-strip telescopes has to comply with the limit in order to be considered as a candidate for prompt proton emission.

For the events discriminated in the way described above the momentum vector of the parent residue (here: ^{58}Cu) is recalculated ignoring the momentum of the proton, which has been identified as a candidate for prompt proton emission. Secondly, the angle Θ (see fig. 3) between the vector of the ^{58}Cu recoil and the pixel in which the low-energy proton had been detected is determined. Thereafter the center-of-mass energy $E_{\mathrm{p,cm}}$ of the proton candidate is recalculated using the new angle Θ and a modified kinetic energy E_{kin} in eq. (1). The kinetic energy is henceforth derived from the kinetic energy of the ^{58}Cu recoil after the target instead of the original kinetic energy of the compound system. Coincident γ-rays are finally used to increment an $E_{\mathrm{p,cm}}$-E_γ correlation matrix. Figure 7 provides two examples of proton center-of-mass energy spectra in coincidence with the 1287 keV $11/2^- \rightarrow 7/2^-$ (panel (a))

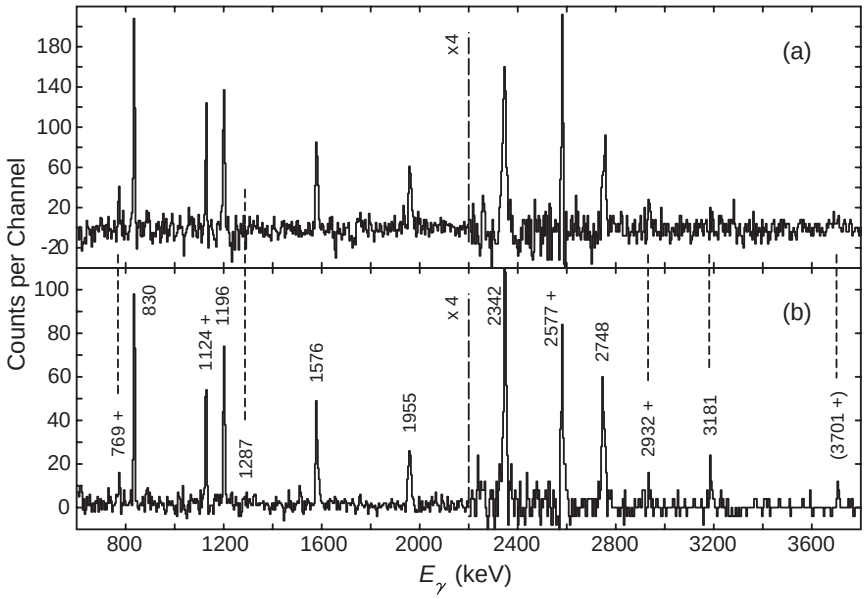

Fig. 9. Gamma-ray spectra of ^{58}Cu in coincidence with the observed proton peak obtained from a proton-γ coincidence matrix (a) and a proton-$\gamma\gamma$ coincidence cube (b). The peak labels are in keV, and a "+" sign marks the transitions in ^{57}Ni. See text for details.

and the 1124 keV $9/2^+ \rightarrow 7/2^-$ (panel (b)) transitions in ^{57}Ni. The overlayed grey spectra in both panels represent the properly normalized total projection of the correlation matrix. Clearly, a proton peak at $E_{\mathrm{p,cm}} \sim 2.3$ MeV is visible in fig. 7(b) with an approximate width of 300 keV. No obvious signs of peaks at either 2.1 or 3.0 MeV are visible in fig. 7(a), which would correspond to the tentative proton branches into the 3864 keV $11/2^-$ state in ^{57}Ni (cf. fig. 5). The kink at 3.2 MeV in both proton spectra of fig. 7 is related to the refined treatment of the low-energy protons (see above).

Figure 8 shows proton center-of-mass energy spectra derived from an $E_{\mathrm{p,cm}}$-E_γ-E_γ correlation cube. On top of the previously described analysis, an additional coincident γ-ray at either 830, 1124, 1197, 1576, 1955, 2342, or 2748 keV (named "band" in fig. 8) is demanded. Figures 8(a) and (b) show the proton spectra in coincidence with any member of the "band" and the 1124 keV $9/2^+ \rightarrow 7/2^-$ transition in ^{57}Ni and the 830 keV $(11^+) \rightarrow (9^+)$ in ^{58}Cu, respectively. The spectrum in fig. 8(c) is in coincidence with any combination of the band members. The measured peak position of $\overline{E}_{\mathrm{p}} = 2290(20)$ keV is in agreement with the expected value of $E_{\mathrm{p}} = 57/58 \cdot Q_{\mathrm{p}} = 2301(5)$ keV. The full-width at half maximum of the peak corresponds nicely to the value estimated in sect. 2 (see eq. (2)).

Combining the counts in figs. 8(a) and (b), the fraction of counts in the proton line amounts to 51(4)% of the total number of counts. This is consistent with a 100% proton branch from the 8915 keV state in ^{58}Cu, in agreement with earlier estimates [1,5]. An independent way of determining the proton branch, b_{p}, from the 8915 keV state is to investigate the ratios R of γ-ray yields in 1α1p1n-gated (Y_1) and 1α2p1n-gated (Y_2) spectra. The procedure is very similar to the one used to derive the branching of the prompt α decay in ^{58}Ni [13]. Using $b_\gamma = 1 - b_{\mathrm{p}}$

$$Y_1 = \epsilon_{\mathrm{p}} \cdot (1 - b_{\mathrm{p}}) + 2\epsilon_{\mathrm{p}}(1 - \epsilon_{\mathrm{p}}) \cdot b_{\mathrm{p}} \tag{4}$$

and

$$Y_2 = {\epsilon_{\mathrm{p}}}^2 \cdot b_{\mathrm{p}}\,, \tag{5}$$

for the 830 and 1124 keV transitions and

$$Y_1' = \epsilon_{\mathrm{p}} \cdot (1 - b_1 + b_1(1 - b_{\mathrm{p}})) + 2\epsilon_{\mathrm{p}}(1 - \epsilon_{\mathrm{p}}) \cdot b_1 b_{\mathrm{p}} \tag{6}$$

and

$$Y_2' = {\epsilon_{\mathrm{p}}}^2 \cdot b_1 b_{\mathrm{p}}\,, \tag{7}$$

for the higher-lying transitions in the rotational band. $\epsilon_{\mathrm{p}} = 0.23(1)$ denotes the proton detection efficiency for single proton hits in the Si-strip telescopes (all protons have to be detected there) for ^{57}Ni final residues, and $b_1 = 0.67(5)$ is the branching of the 830 keV transition in the decay of the 9745 keV state. With $R = Y_1/Y_2$ and $R' = Y_1'/Y_2'$ one obtains

$$b_{\mathrm{p}} = \frac{1}{\epsilon_{\mathrm{p}}(R+2) - 1} \quad \text{and} \quad b_{\mathrm{p}} b_1 = \frac{1}{\epsilon_{\mathrm{p}}(R'+2) - 1}, \tag{8}$$

respectively. The γ-ray analysis yields an average $R = 6.8(8)$ for the 830 and 1124 keV transitions, and $R' = 8.7(9)$ for the 1197, 1576, 1955, 2342, and 2748 keV transitions. The weighted mean value of the results from eq. (8) provides $b_{\mathrm{p}} = 1.00(^{18}_{12})$, which strongly supports the idea of an exclusive proton decay of the 8915 keV state in ^{58}Cu.

Instead of looking at γ-gated proton spectra, the improved sensitivity of the proton lines allows also to investigate proton-gated γ-ray spectra. This is illustrated in fig. 9, which shows γ-ray spectra in coincidence with 2.1 MeV $< E_{\mathrm{p,cm}} <$ 2.5 MeV proton (panel (a)) and in additional coincidence with one of the previously mentioned "band" members (panel (b)). Both spectra reveal

peaks exclusively at γ-ray energies which are associated with the prompt proton decay of the 8915 keV state in ^{58}Cu. In fig. 9(b) the peak-to-background ratio is further improved compared to fig. 9(a), which of course is due to the additional γ-coincidence condition. Two results have to be stressed: Firstly, there is no evidence for the 1287 keV transition in ^{57}Ni. Once more, this speaks in favour of an exclusive decay into the 3701 keV $9/2^+$ state of ^{57}Ni. Secondly, a weak but clean (fig. 9(b)) peak is seen at 3701 keV. Since the energy lies some 50 keV above an expected, possible continuation of the rotational band in ^{58}Cu and because it exactly matches the excitation energy of the daughter state in ^{57}Ni, we tentatively assign this peak to a weak $E3$ branch from the $9/2^+$ state into the $3/2^-$ ground state of ^{57}Ni. This would be consistent with early γ-ray studies of ^{57}Ni [24].

4 Discussion

The present information on the prompt proton decay in ^{58}Cu can be summarized as follows:

- The existing data is consistent with a single proton line between the 8915 keV state in ^{58}Cu and the 3701 keV state in ^{57}Ni.
- There is no evidence for γ-ray transitions competing with the proton decay. A conservative lower limit for the proton branching from the 8915 keV state is 93% from the present study.
- The spin and parity of the initial state is (9^+), and it is $9/2^+$ for the final state [12].
- The lifetime of the 8915 keV state is 0.06 ps $< \tau <$ 0.58 ps [13].
- Individual lifetimes of other band members [6] and an average quadrupole measurement of the band [1] consistently yield a deformation of the band of $\beta_2 \sim 0.37$–0.40 (assuming axial symmetry).
- The configuration of the ^{58}Cu band is unique: It is based on a generic four-particle four-hole (4p-4h) excitation across the shell gap at particle numbers $N, Z =$ 28, and it involves one proton and one neutron in the $1g_{9/2}$ intruder orbit [1,25].

At present, a theoretical model is unfortunately not at hand, which can account for the dynamics of the shape change associated with the decay mode of prompt proton emission and the overlap of the wave functions of the initial deformed and final near spherical states. Stationary approaches using either simple semiclassical WKB estimates, which assume spherical initial and final states, or advanced methods used to describe deformed ground-state proton emitters [8] predict similar halflives on the order of 10^{-4} ps for the proton decay in ^{58}Cu, which imply an experimental spectroscopic factor of $\sim 10^{-3}$ [13].

If one associates this hindrance with the tunneling through the barrier between the well-deformed and spherical states in ^{58}Cu, one may quest the potential impact of the prompt particle decays concerning the decay-out process from superdeformed bands, *i.e.* whether they are due

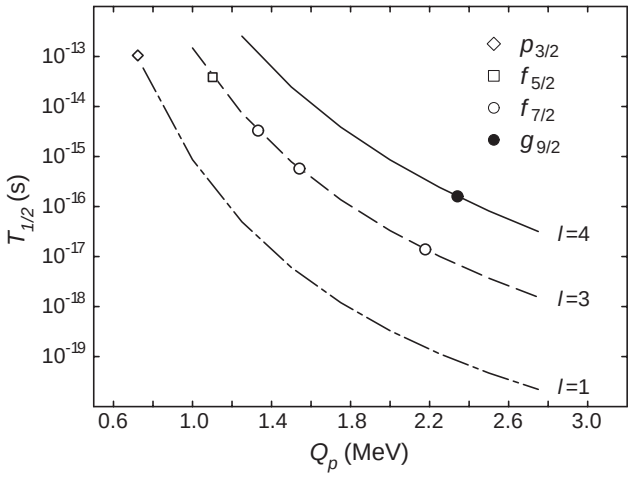

Fig. 10. Estimates of halflives for protons emitted from ^{58}Cu with angular momenta $l = 1$, 3, or 4 $\hbar$ as a function of the Q-value of the decay. The formalism of ref. [26] has been applied. The symbols mark the energies of possible proton decays into known $9/2^+$ (filled circle), $11/2^-$ (open circles), $13/2^-$ (open square), and $15/2^-$ (open diamond) states in ^{57}Ni.

to accidentally enhanced random matrix elements or governed by selection rules in the $A \sim 60$ region. Figure 10 presents semiclassical WKB estimates of halflives of proton emission from spherical states into spherical states with different angular momenta l from ^{58}Cu into ^{57}Ni as a function of the Q-value. The WKB model, of course, does not include any nuclear-structure information. For a given isotope, the calculated decay rates depend solely on the Q-value and the angular momentum of the emitted proton. Any distinct difference between these simple estimates and the observations can be taken as a sign of the importance of selection rules in the decay-out process. A statistical process through the coupling to highly excited states in the normally deformed minimum, which may comprise compound-state components, would spread the decay strengths over all possible, final states in ^{57}Ni. Since these decay strengths have to be weighted with proton energy and proton angular momentum, this scenario should by and large follow the WKB predictions.

The symbols in fig. 10 indicate energetically possible proton decays of the 8915 keV (9^+) state into known $9/2^+$, $11/2^-$, $13/2^-$, and $15/2^-$ states in ^{57}Ni. Two things are worth mentioning: First of all, the halflife prediction of $T_{1/2} = 2 \cdot 10^{-4}$ ps for the observed $1g_{9/2}$ decay is consistent with previous WKB calculations (cf. ref. [1,13]). The second conclusion from fig. 10 is that the proton decay should proceed into the yrast 3864 keV $11/2^-$ state in ^{57}Ni, which is included in fig. 5. This is totally at variance with the observations. This $l = 3$ $1f_{7/2}$ proton decay is predicted to be about ten times faster than the observed decay into the 3701 keV $9/2^+$ state. Even the decay into the yrare $11/2^-$ state is competitive to the observed $l = 4$ decay. This discrepancy between the simple model and the observations hints at nuclear-structure effects, which are necessary to counteract the preference of the $1f_{7/2}$ decay strengths. It is difficult to attribute the exclusive $1g_{9/2}$

branch to a single, accidentally enhanced random matrix element, not least because of similar observations and situations in the neighbouring isotope ^{59}Cu [3,4] —all known prompt proton decays are of $1g_{9/2}$ character.

One issue is the overlap of the initial and final wave functions. Starting from a 4p-4h $\pi(1g_{9/2}) \otimes \nu(1g_{9/2})$ configuration, the emission of the $1g_{9/2}$ proton naturally leads to the $1g_{9/2}$ neutron single-particle state in ^{57}Ni, if in the course of the shape change the 4p-4h excitation within the fp shell would be reconfigured. On the contrary, a presumed $1f_{7/2}$ proton decay would create an additional hole in the $1f_{7/2}$ shell and keep the two particles in the $1g_{9/2}$ shell. Taking into account the same 4p-4h recoupling in the course of the decay, a $1f_{7/2}$ decay needs a coupling to a $\pi(1f_{7/2})^{-1} \otimes \pi(1g_{9/2}) \otimes \nu(1g_{9/2})$ partition in the wave function of the $11/2^-$ state. This partition, however, must be extremely small, because the energies which are necessary to create an extra hole in the $1f_{7/2}$ shell and excite two particles into the $1g_{9/2}$ orbit each amount to several MeV.

The second issue is related to the deformation change in the course of the decay. A recent extensive study of multiple deformed and superdeformed bands in the neighbouring nucleus ^{59}Cu provided evidence that the deformation parameter ε_2 of the rotational bands in the $A \sim 60$ region can be parametrized with

$$\varepsilon_2 \approx 0.09 + 0.04 \cdot q, \tag{9}$$

where q is the sum of holes in the $1f_{7/2}$ orbit and particles in the $1g_{9/2}$ orbit [27]. The band in ^{58}Cu has $q = 6$, *i.e.* $\beta_2 \approx 1.05 \cdot \varepsilon_2 \approx 0.35$, which is in agreement with the measurements. While the emission of a $1g_{9/2}$ proton reduces q, the emission of a $1f_{7/2}$ proton would increase q. Since the decay has to proceed from a highly deformed into a spherical state, the former decay is clearly favourable. In addition, the single-step γ-ray linking transitions at 4171 and 4399 keV have $B(E2)$ strengths on the order of 10^{-4} to 10^{-5} compared to the 830 keV in-band transition [6]. This yields a hindrance factor that is about one order of magnitude larger than the hindrance factor deduced from the experimental spectroscopic factor of the proton decay. Assuming that the final state of the 4171 keV decay has a dominating spherical $\pi(1g_{9/2}) \otimes \nu(1g_{9/2})$ partition (cf. ref. [19]), this single-step process should have an overlap between the initial and final wave function comparable to the observed $1g_{9/2}$ proton decay. Thus, the reduced hindrance of the latter compared to the 4171 keV may be due the inherent decrease of q and, hence, deformation when the proton is emitted.

5 Summary

A first dedicated experiment aiming at in-beam high-resolution particle-γ coincidence spectroscopy has been performed. The present revised study of the first case of the new decay mode of prompt proton particle emission in ^{58}Cu (along with the results from ref. [13]) clearly demonstrates the feasibility of such experiments with present-day instrumentation. Further evidence has been presented which supports the idea of an exclusive 100% proton branch from the 8915 keV (9^+) state located in the second minimum of ^{58}Cu into the 3701 keV $9/2^+$ neutron single-particle state in ^{57}Ni. Simple estimates of proton emission halflives indicate that the proton decay likely follows selection rules related to the deformation and the quantum numbers of the initial and final states. Future investigations of the prompt proton decay in ^{58}Cu are going to focus on angular distributions and correlations of the emitted protons and γ-rays. They may shed light on both the initial wave function of the emitted $1g_{9/2}$ proton and the timing of the drastic shape change associated with this unique two-dimensional quantum tunneling process [28,29]. Furthermore, the sensitivity of the present experiment allows for a survey of particle-decaying states in the $A \sim 60$ region.

The authors thank J. Sørensen and G. Sletten for the target preparation, B. Blank for discussions, and M.P. Carpenter, S. Freeman, T. Lauritsen, M. Leddy, C.J. Lister, and R. De Souza for support concerning GAMMASPHERE, the neutron detectors, and the silicon-strip array, respectively. This research was supported in part by the Swedish Research Council, the U.S. Department of Energy under contracts No. DE-FG05-88ER40406 (WU) and No. W-31-109-ENG38 (ANL), the U.S. National Science Foundation under grant No. PHY95-14157 (Penn), and the German BMBF under contract No. 06 OK 958. ORNL is managed by UT-Batelle, LLC, for the U.S. Department of Energy under contract No. DE-AC05-00OR22725.

References

1. D. Rudolph, C. Baktash, W. Nazarewicz, W. Satula, M.J. Brinkman, M. Devlin, H.-Q. Jin, D.R. LaFosse, L.L. Riedinger, D.G. Sarantites, C.H. Yu, Phys. Rev. Lett. **80**, 3018 (1998).
2. D. Rudolph, C. Baktash, M.J. Brinkman, E. Caurier, D.J. Dean, M. Devlin, J. Dobaczewski, P.-H. Heenen, H.-Q. Jin, D.R. LaFosse, W. Nazarewicz, F. Nowacki, A. Poves, L.L. Riedinger, D.G. Sarantites, W. Satula, C.H. Yu, Phys. Rev. Lett. **82**, 3763 (1999).
3. C. Andreoiu, D. Rudolph, C. Fahlander, A. Gadea, D.G. Sarantites, C.E. Svensson, in *Proceedings of the International Workshop Pingst 2000 – Selected Topics on $N = Z$ Nuclei, June 2000, Lund, Sweden*, edited by D. Rudolph, M. Hellström (Bloms i Lund AB, 2000) p. 21.
4. D. Rudolph, C. Andreoiu, C. Fahlander, R.J. Charity, M. Devlin, D.G. Sarantites, L.G. Sobotka, D.P. Balamuth, J. Eberth, A. Galindo-Uribarri, P.A. Hausladen, D. Seweryniak, Th. Steinhardt, to be published in Phys. Rev. Lett.
5. D. Rudolph, C. Baktash, M. Devlin, D.R. LaFosse, L.L. Riedinger, D.G. Sarantites, C.-H. Yu, Phys. Rev. Lett. **86**, 1450 (2001).
6. D. Rudolph, C. Fahlander, A. Algora, C. Andreoiu, R. Cardona, C. Chandler, G. de Angelis, E. Farnea, A. Gadea, J. Garcés Narro, J. Nyberg, M. Palacz, Zs. Podolyak,

T. Steinhardt, O. Thelen, Phys. Rev. C **63**, 021301(R) (2001).
7. S. Åberg, P.B. Semmes, W. Nazarewicz, Phys. Rev. C **56**, 1762 (1997).
8. E. Maglione, L.S. Ferreira, R.J. Liotta, Phys. Rev. Lett. **81**, 538 (1998).
9. P. Talou, N. Carjan, D. Strottman, Nucl. Phys. A **647**, 21 (1999).
10. C.N. Davids, H. Esbensen, Phys. Rev. C **61**, 054302 (2000).
11. A.T. Kruppa, B. Barmore, W. Nazarewicz, T. Vertse, Phys. Rev. Lett. **84**, 4549 (2000).
12. D. Rudolph, D. Weisshaar, F. Cristancho, J. Eberth, C. Fahlander, O. Iordanov, S. Skoda, Ch. Teich, O. Thelen, H.G. Thomas, Eur. Phys. J. A **6**, 377 (1999); D. Rudolph, in *Proceedings of the International Conference on Achievements and Perspectives in Nuclear Structure, July 1999, Crete, Greece*, edited by S. Åberg, C. Kalfas, Phys. Scr. T **88**, 21 (2000).
13. D. Rudolph, A. Gadea, G. de Angelis, C. Fahlander, A. Algora, C. Andreoiu, R. Cardona, C. Chandler, E. Farnea, J. Garcés Narro, J. Nyberg, M. Palacz, Zs. Podolyak, T. Steinhardt, O. Thelen, Nucl. Phys. A **694**, 132 (2001).
14. I.-Y. Lee, Nucl. Phys. A **520**, 641c (1990).
15. D.G. Sarantites, P.-F. Hua, M. Devlin, L.G. Sobotka, J. Elson, J.T. Hood, D.R. LaFosse, J.E. Sarantites, M.R. Maier, Nucl. Instrum. Methods A **381**, 418 (1996).
16. MICROBALL, `http://wunmr.wustl.edu/~dgs/mball`.
17. B. Davin, R.T. de Souza, R. Yanez, Y. Larochelle, R. Alfaro, H.S. Xu, A. Alexander, K. Bastin, L. Beaulieu, J. Dorsett, G. Fleener, L. Gelovani, T. Lefort, J. Poehlman, R.J. Charity, L.G. Sobotka, J. Elson, A. Wagner, T.X. Liu, X.D. Liu, W.G. Lynch, L. Morris, R. Shomin, W.P. Tan, M.B. Tsang, G. Verde, J. Yurkon, Nucl. Instrum. Methods A **473**, 302 (2001).
18. J.F. Ziegler, J.P. Biersack, *The Stopping and Range of Ions in Solids* (Pergamon Press, New York, 1985); associated computer code TRIM96.
19. D. Rudolph, C. Baktash, M.J. Brinkman, M. Devlin, H.-Q. Jin, D.R. LaFosse, L.L. Riedinger, D.G. Sarantites, C.-H. Yu, Eur. Phys. J. A **4**, 115 (1999).
20. D.C. Radford, Nucl. Instrum. Methods Phys. Res. A **361**, 297 (1995).
21. J. Theuerkauf, S. Esser, S. Krink, M. Luig, N. Nicolay, O. Stuch, H. Wolters, program TV, University of Cologne, unpublished.
22. K.S. Krane, R.M. Steffen, R.M. Wheeler, At. Data Nucl. Data Tables **11**, 351 (1973).
23. C.E. Svensson, J.A. Cameron, S. Flibotte, G. Gervais, D.S. Haslip, J.M. Nieminen, J.C. Waddington, J.N. Wilson, G.C. Ball, A. Galindo-Uribarri, V.P. Janzen, D.C. Radford, D. Ward, M. Cromaz, T.E. Drake, Nucl. Instrum. Methods A **396**, 288 (1997).
24. C.R. Gould, D.P. Balamuth, P.F. Hinrichsen, R.W. Zurmühle, Phys. Rev. **188**, 1792 (1969).
25. A.V. Afanasjev, I. Ragnarsson, P. Ring, Phys. Rev. C **59**, 3166 (1999).
26. A.R. Barnett, Comput. Phys. Commun. **27**, 147 (1982).
27. C. Andreoiu, D. Rudolph, I. Ragnarsson, C. Fahlander, R.A.E. Austin, M.P. Carpenter, R.M. Clark, J. Ekman, R.V.F. Janssens, T.L. Khoo, F. Kondev, T. Lauritsen, T. Rodinger, D.G. Sarantites, D. Seweryniak, T. Steinhardt, C.E. Svensson, O. Thelen, J.C. Waddington, to be published in Eur. Phys. J. A.
28. P. Talou, in *Proceedings of the International Workshop Pingst 2000 – Selected Topics on $N = Z$ Nuclei, June 2000, Lund, Sweden*, edited by D. Rudolph, M. Hellström (Bloms i Lund AB, 2000) p. 10.
29. S.G. Kadmensky, A.A. Sonzogni, Phys. Rev. C **62**, 054601 (2000).